Supporting Information

Functional nucleic acid probe for parallel monitoring K^+ and protoporphyrin IX in living organisms

Hanjun Cheng[1,4], Xuefeng Qiu[2], Xiaozhi Zhao[2], Wei Meng[3], Da Huo[1] and Hui Wei[1,*]

[1]Department of Biomedical Engineering, College of Engineering and Applied Sciences, Collaborative Innovation Center of Chemistry for Life Sciences, Nanjing National Laboratory of Microstructures, Nanjing, Jiangsu, 210093, China Nanjing, Jiangsu, 210093, China.

[2]Department of Urology, Nanjing Drum Tower Hospital, the Affiliated Hospital of Nanjing University Medical School, Nanjing, Jiangsu, 210008, China.

[3]School of Physics, Collaborative Innovation Center of Advanced Microstructures, Nanjing National Laboratory of Microstructures, Nanjing University, Nanjing, Jiangsu, 210093, China.

[4]State Key Laboratory of Analytical Chemistry for Life Science, Nanjing University, Nanjing 210093, China.

Email: weihui@nju.edu.cn; Fax:+86-25-83594648; Tel: +86-25-83593272; http://weilab.nju.edu.cn.

Table of contents

10 uM PPIX, 2.5 mM EDTA and 100 mM Na^+. PPIX detection was performed with **solution 2** containing 10 uM Probe G, 100 mM K^+, 250 nM PPIX and 2.5 mM EDTA. Error bars indicate standard deviations of three independent measurements. Note: Ringer sol. ≡ Ringer's solution; mix. ≡ mixture.

Figure S6. Fluorescence responses of 10 μM Probe G-PPIX complex in the presence of 100 mM Na^+ and 10 mM K^+ (**1**) and 150 mM Na^+ and 10 mM K^+ (**2**).

Figure S7. Evaluation of potential cross-talk between parallel detection of K^+ (A) and PPIX (B). Error bars indicate standard deviations of three independent measurements.

Figure S8. Typical fluorescence responses to PPIX in living brain microdialysates with (red curve) and without (black curve) the Probe G.

Figure S9. Typical HPLC chromatograms of different porphyrins.

Figure S10. Typical HPLC chromatogram of the microdialysate from living brains.

Figure S11. Typical fluorescence responses to PPIX in living brain microdialysates with (red curve) and without (black curve) the Probe G.

Figure S12. Dynamic changes of PPIX in tumor-bearing (red bars) or healthy (black bars) mice before and after the administration of 5-ALA. Data are presented as mean ± SD.

Figure S13. PPIX content in glioma-bearing mice before (column 1) and after (column 2) the administration of 5-ALA. Data are presented as mean ± SD.

Referneces

K^+ / mM	Current method	ICP-AAS
Rat 1	1.95	1.83
Rat 2	1.51	1.40
Rat 2	1.67	1.56

Table S1. Measurements of K^+ concentrations in brain microdialysates of living rats determined by the current method and by inductive coupled plasma atomic absorption spectrophotometry (ICP-AAS).

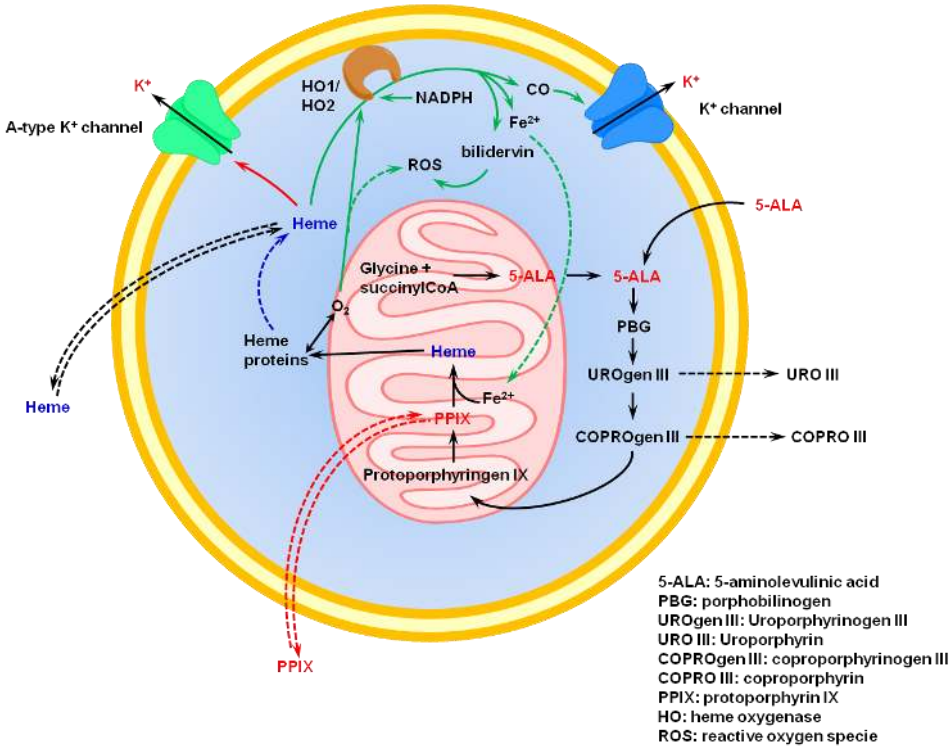

Figure S1. Scheme of the potential linkage among the cellular pathways involved K^+ and PPIX.[1-13]

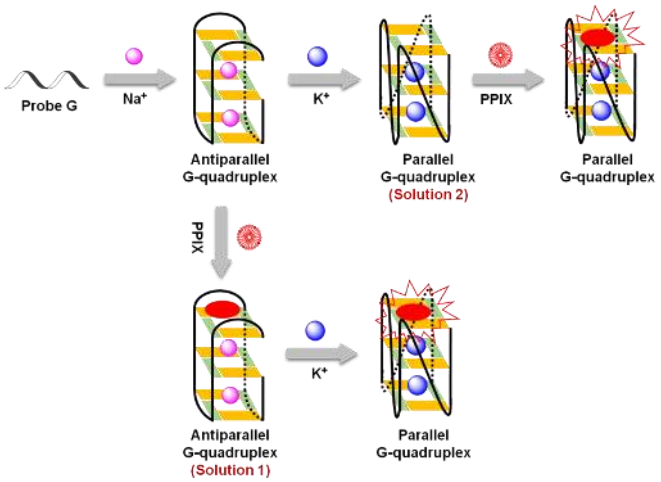

Figure S2. Schematic illustration of K^+-induced antiparallel-to-parallel conformational transition of the G-quadruplex and the remarkable fluorescence enhancement of PPIX by the parallel G-quadruplex for K^+ and PPIX detection.

K^+-induced Conformation Transition of Probe G for PPIX Fluorescence Enhancement. The K^+-induced antiparallel-to-parallel conformational transition of the selected 18-mer Probe G, the interaction between G-quadruplexes and PPIX, and the remarkable fluorescence enhancement of PPIX by the formed parallel G-quadruplex were studied by circular dichroism (CD), UV-visible absorption and fluorescent spectroscopy (Figures S2 and S3).[14] The antiparallel-to-parallel structure transition was evidenced by the corresponding CD spectra, as shown in Figure S3A. In the presence of 200 mM Na^+, Probe G exhibited two characteristic bands of antiparallel G-quadruplexes (i.e., one positive band at 295 nm and one negative band at 265 nm), indicating that Probe G folded into an antiparallel quadruplex structure.[15] With the further addition of K^+ into the Na^+-contained Probe G solution, the positive band at 295 nm gradually decreased until disappear whilst the negative band at 265 nm became more and more positive, suggesting the gradual transition of G-quadruplex structure from antiparallel ones into parallel ones.

The interactions between the formed G-quadruplexes and PPIX as well as the fluorescence enhancement of PPIX by the G-quadruplexes were then investigated by using UV-visible and fluorescent spectroscopy. As shown in Figures S3B and S3C, neither absorption bands (350-500 nm range) nor fluorescent emission peaks (500-800 nm range) were observed for Probe G. PPIX, on the other hand, exhibited a broaden absorption peak at around 460 nm, suggesting a severe aggregation of PPIX in aqueous solution. The aggregation of PPIX resulted in its weak but characteristic fluorescent emission (one sharp peak at 628 nm and the other broad emission band from 655 nm to 720 nm). The formation of complex between the antiparallel G-quadruplex and PPIX led to a 5-nm blue shift and a 1.3-fold hyperchromicity of PPIX absorption band. The fluorescence of PPIX also showed a 1.3-fold enhancement with a red shift of its fluorescent emission peaks (i.e., from 628 nm to 635 nm). Such changes indicated weak interactions between the antiparallel G-quadruplex and PPIX. In contrast, the formation of complex between the K^+-induced parallel G-quadruplex and PPIX resulted in a more significant hyperchromicity in the Soret band of PPIX (1.9 fold), accompanying with a remarkably enhanced fluorescence of PPIX (9.0 fold). Such strong interactions between the parallel G-quadruplex and PPIX might be originated from the hydrophobic and π-π stacking interactions. The remarkable promotion of PPIX fluorescence upon binding to the K^+-induced parallel G-quadruplex encouraged us to use the Probe G-based parallel G-quadruplex as an effective probe for parallel detection of K^+ and PPIX in living organisms.

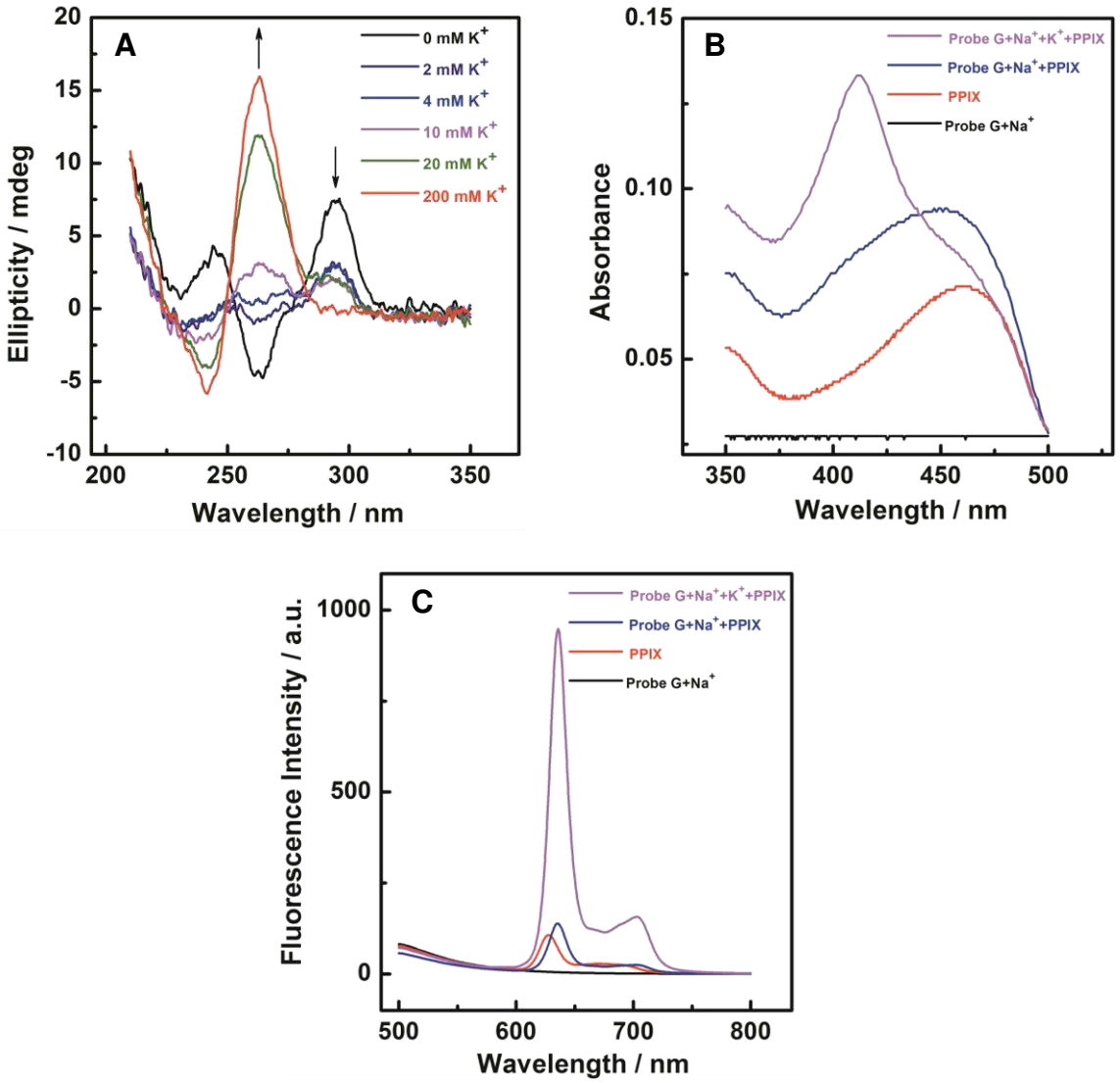

Figure S3. (A) CD spectra of 20 μM Probe G in the presence of 100 mM Na^+ and different concentrations of K^+ (0, 2, 4, 10, 20, and 200 mM). UV-visible absorption spectra (B) and fluorescence spectra (C) of 10 μM Probe G in the presence of 100 mM Na^+ (black curve), 10 μM PPIX (red curve), 10 μM Probe G-PPIX complex in the presence of 100 mM Na^+ (blue curve), and 10 μM Probe G-PPIX complex in the presence of 100 mM Na^+ and 100 mM K^+ (magenta curve).

Note: a weak shoulder peak was observed at around 410 nm for the 10 μM Probe G-PPIX complex in the presence of 100 mM Na^+ (blue curve in Figure S3B), which may be responsible for the Na^+-induced fluorescence shift and enhancement (blue curve in Figure S3C).

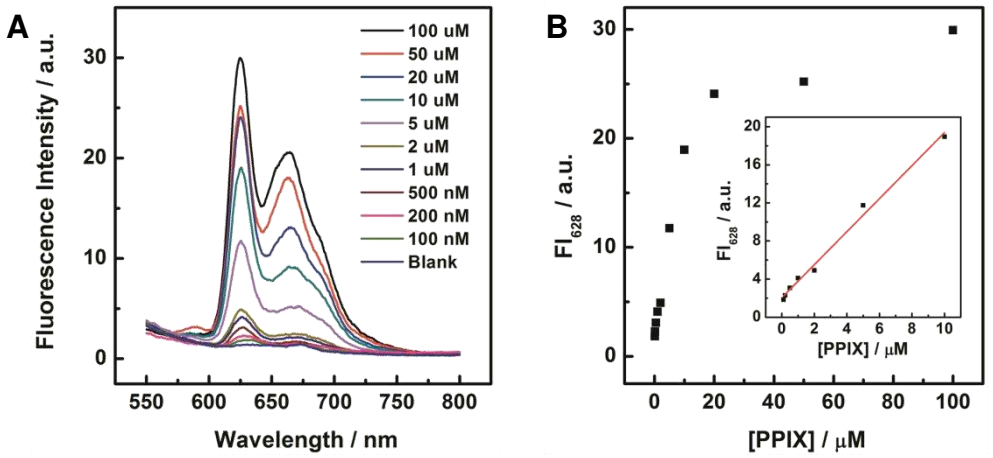

Figure S4. (A) Typical fluorescence responses of pristine PPIX in 0.10 M Tris-HCl buffer (pH 7.0). (B) Dependence of PPIX fluorescence intensity on PPIX concentrations. Inset: Plot of FI_{628} against PPIX concentration. FI_{628} represents the fluorescence intensity at 628 nm.

As shown in Figure S4A, the fluorescent intensity of pristine PPIX was much lower when compared to PPIX complexed by the G-quadruplex. More, it showed a linear response toward PPIX concentration ranging only from 100 nM to 10 μM (Figure 4B), which was narrower than that of PPIX complexed by the G-quadruplex. These results demonstrated that it is necessary to use the G-quadruplex probe for sensitive detectin of PPIX.

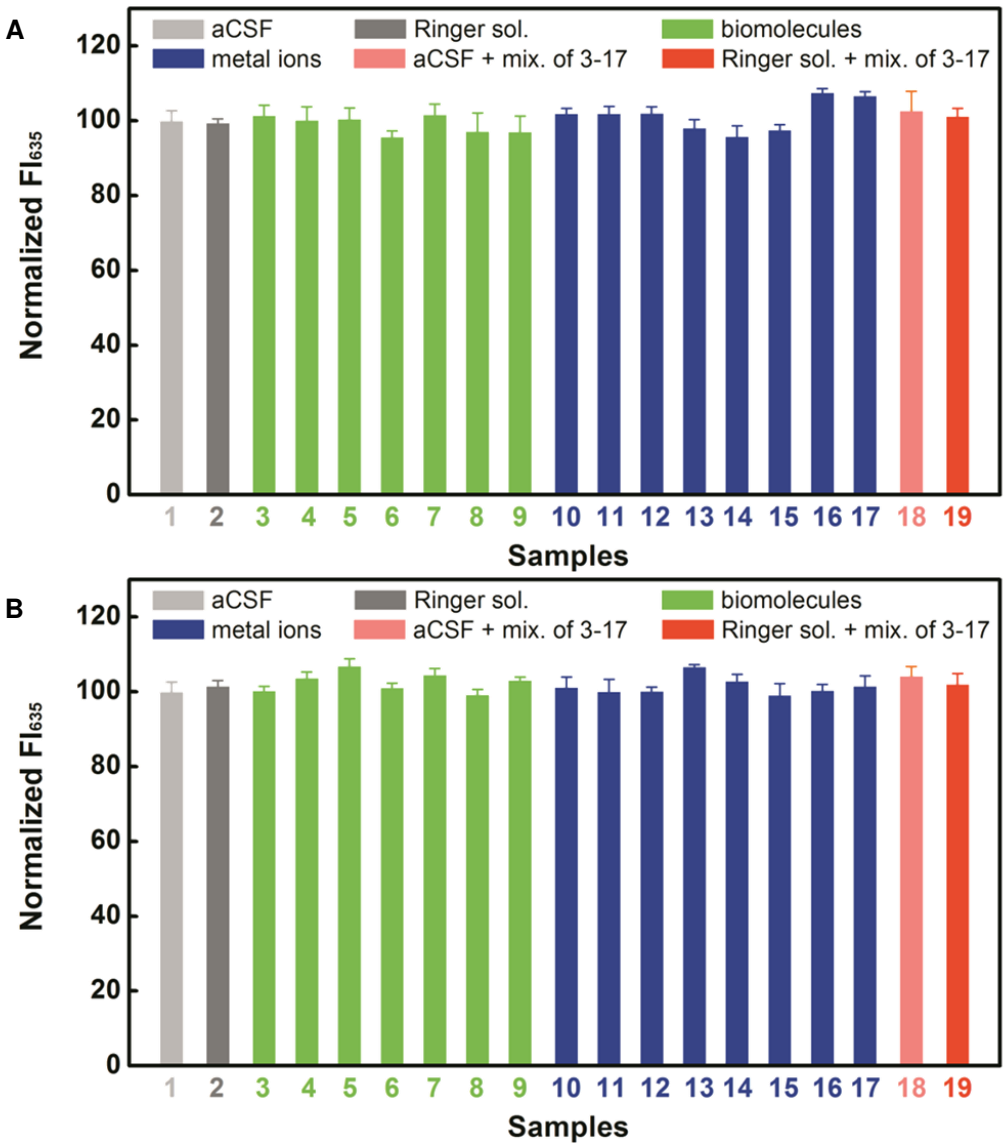

Figure S5. Selective detection of 2 mM K^+ (A) and 250 nM PPIX (B) in the absence and presence of potential interfering components. From **1** to **19** are aCSF (**1**), Ringer's solution (**2**), 500 μM glucose (**3**), 500 μM lactate (**4**), 10 μM AA (**5**) , 10 μM 5-HT (**6**), 10 μM UA (**7**), 10 μM DA (**8**), 10 μM DOPAC (**9**), 1 mM Ca^{2+} (**10**), 1 mM Mg^{2+} (**11**), 10 μM Co^{2+} (**12**), 10 μM Mn^{2+} (**13**), 10 μM Fe^{2+} (**14**), 10 μM Fe^{3+} (**15**), 10 μM Cu^{2+} (**16**), 10 μM Zn^{2+} (**17**), mixture of aCSF and 3-17 (**18**), mixture of Ringer's solution and 3-17 (**19**), respectively. K^+ detection was performed with **solution 1** containing 10 uM Probe G, 10 uM PPIX, 2.5 mM EDTA and 100 mM Na^+. PPIX detection was performed with **solution 2** containing 10 uM Probe G, 100 mM K^+, 250 nM PPIX and 2.5 mM EDTA. Error bars indicate standard deviations of three independent measurements. Note: Ringer sol. ≡ Ringer's solution; mix. ≡ mixture.

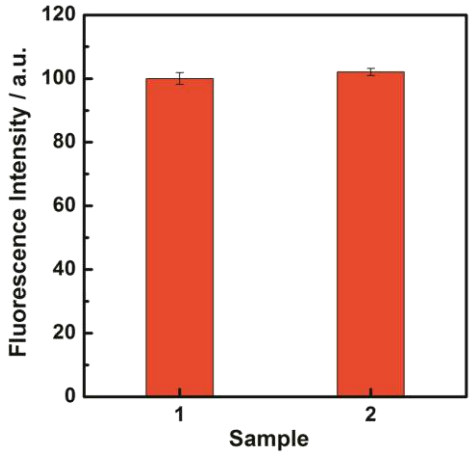

Figure S6. Fluorescence responses of 10 μM Probe G-PPIX complex in the presence of 100 mM Na^+ and 10 mM K^+ (**1**) and 150 mM Na^+ and 10 mM K^+ (**2**).

As shown in Figure S6, the large fluctuation of Na^+ concentration (i.e., from 100 mM to 150 mM) did not signficantly affect the flurescence response of the detection system. Such Na^+-independent response essentially allows the current detection technique for parallel monitoring K^+ and PPIX during complicated biological processes, in which the concentration of Na^+ may undergo dramatic changes.

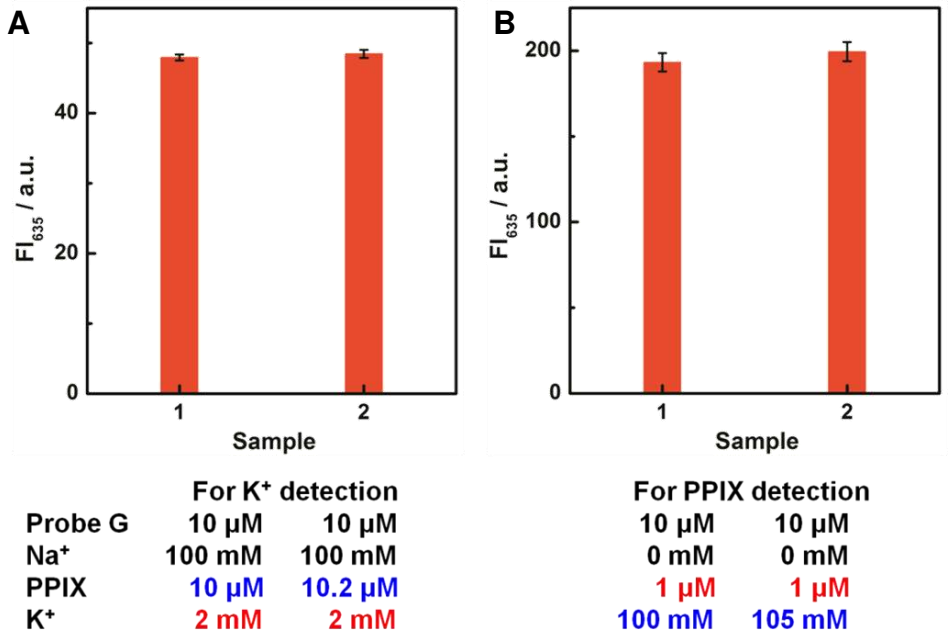

Figure S7. Evaluation of potential cross-talk between parallel detection of K^+ (A) and PPIX (B). Error bars indicate standard deviations of three independent measurements.

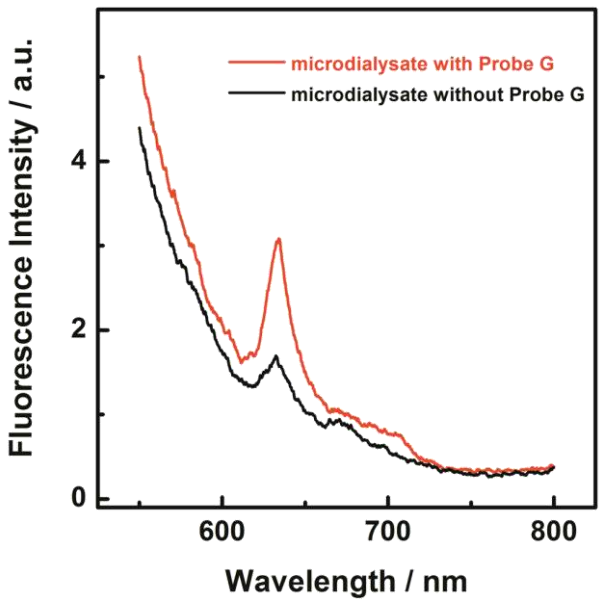

Figure S8. Typical fluorescence responses to PPIX in living brain microdialysates with (red curve) and without (black curve) the Probe G.

As shown in Figure S8, the Probe G significantly enhanced the fluorescence of PPIX, which enabled the sensitively monitoring PPIX in living brain microdialysates.

About other porphyrins. Besides PPIX, there are other porphyrins (such as uroporphyrins and coproporphyrins) in the living organisms (Figure S1). These porphyrins have similar structures with PPIX. They can also interact with the G-quadruplex and thus produce enhanced fluorescent emissions. Therefore, we have identified PPIX as well as uroporphyrin and coproporphyrin in the microdialysate from living brains and tumors with HPLC.

First, we determined the retention times and detection limits of porphyrin standards (Figure S9). The retention times of the HPLC for PPIX, uroporphyrin I, coproporphyrin I, and coproporphyrin III were 3.79 min, 1.25 min, 1.34 min, and 1.35 min, respectively. The estimated detection limits for PPIX, uroporphyrin I, coproporphyrin I, and coproporphyrin III were 500 nM, 4.2 μM, 137 nM, and 31 nM, respectively. The detection limit of HPLC for PPIX was much higher than our method (500 nM vs 0.5 nM).

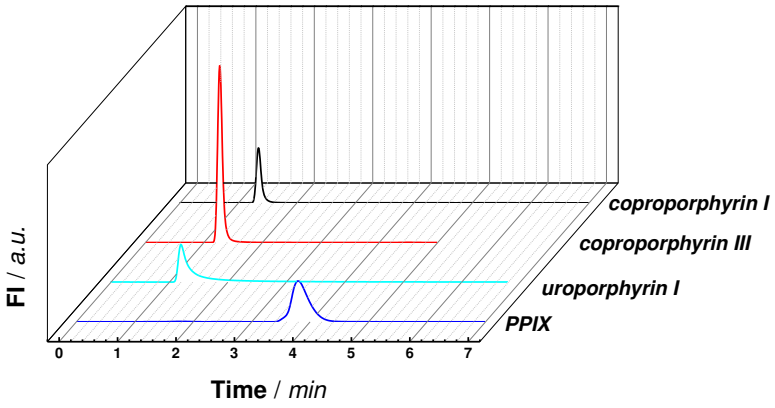

Figure S9. Typical HPLC chromatograms of different porphyrins.

Then, we analyzed the microdialysate samples from living brains and tumors with HPLC. As shown in Figure S10, neither PPIX nor other porphyrins were detected in the microdialysate from living brains with HPLC, which was probably due to the extremely low concentrations of the porphyrins in the living brains and the limited sensitivity of the HPLC used. On the other hand, with our current method both the concentration and dynamic change of PPIX have been successfully measured in the living brains, showing the enhanced sensitivity and much improved analytical performance of our proposed method.

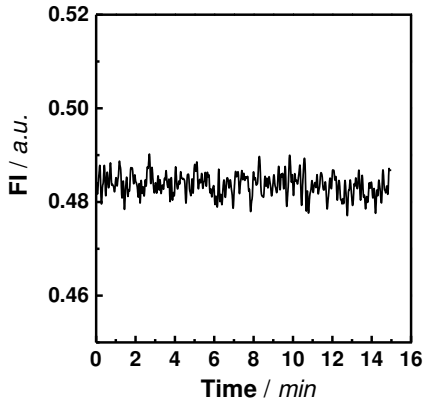

Figure S10. Typical HPLC chromatogram of the microdialysate from living brains.

As shown in Figure S11, both PPIX and other porphyrins were detected in the microdialysate from tumors with HPLC. (Note: due to the very close retention times, uroporphyrins and coproporphyrins cannot be separated from each other with the HPLC used.) And the estimated concentration of PPIX was around 750 nM while certain concentrations of other porphyrin mixtures were also observed.

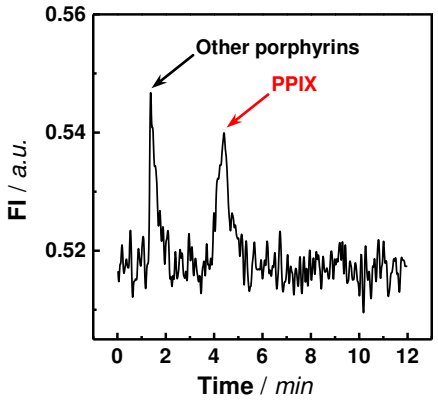

Figure S11. Typical fluorescence responses to PPIX in living brain microdialysates with (red curve) and without (black curve) the Probe G.

Since the fluorescent emission profiles of these porphyrins (including PPIX) are very similar with each other, they cannot be distinguished from each other using our G-quadruplex probe. On the other hand, for biomedical applications (such as photodynamic therapy or image-guided surgery), there is no need to distinguish these porphyrins from each other since all of them are the active species.

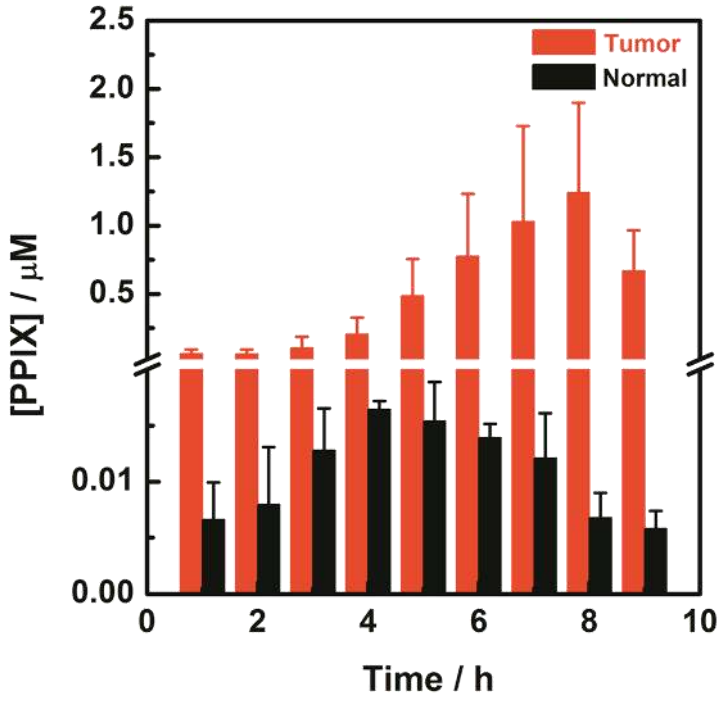

Figure S12. Dynamic changes of PPIX in tumor-bearing (red bars) or healthy (black bars) mice before and after the administration of 5-ALA. Data are presented as mean ± SD.

Since the PPIX levels of healthy mice were very low, to clearly show their dynamic change before and after the administration of 5-ALA, Figure 6B was re-plotted as Figure S12.

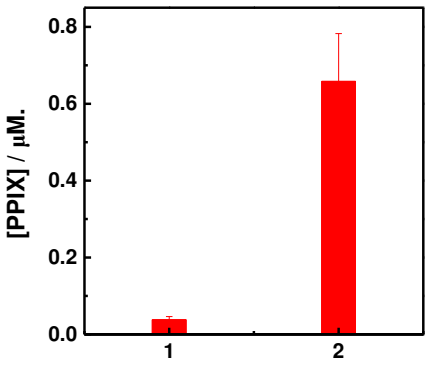

Figure S13. PPIX content in glioma-bearing mice (U87 cell line) before (column 1) and after (column 2) the administration of 5-ALA. Data are presented as mean ± SD.

Referneces

(1) Willis, D.; Moore, A. R.; Frederick, R.; Willoughby, D. A. *Nat. Med.* **1996**, *2*, 87-90.
(2) Hebeda, K. M.; Saarnak, A. E.; Olivo, M.; Sterenborg, H.; Wolbers, J. G. *Acta Neurochirur.* **1998**, *140*, 503-512.
(3) Dore, S.; Goto, S.; Sampei, K.; Blackshaw, S.; Hester, L. D.; Ingi, T.; Sawa, A.; Traystman, R. J.; Koehler, R. C.; Snyder, S. H. *Neuroscience* **2000**, *99*, 587-592.
(4) Nietsch, H. H.; Roe, M. W.; Fiekers, J. F.; Moore, A. L.; Lidofsky, S. D. *J. Biol. Chem.* **2000**, *275*, 20556-20561.
(5) Ningaraj, N. S.; Rao, M.; Hashizume, K.; Asotra, K.; Black, K. L. *J. Pharmacol. Exp. Ther.* **2002**, *301*, 838-851.
(6) Dietze, A.; Berg, K. *Photodiagnosis Photodyn. Ther.* **2005**, *2*, 299-307.
(7) Valdes, P. A.; Leblond, F.; Kim, A.; Harris, B. T.; Wilson, B. C.; Fan, X.; Tosteson, T. D.; Hartov, A.; Ji, S.; Erkmen, K.; Simmons, N. E.; Paulsen, K. D.; Roberts, D. W. *J. Neurosurg.* **2011**, *115*, 11-17.
(8) Wachowska, M.; Muchowicz, A.; Firczuk, M.; Gabrysiak, M.; Winiarska, M.; Wanczyk, M.; Bojarczuk, K.; Golab, J. *Molecules* **2011**, *16*, 4140-4164.
(9) Liao, H.; Noguchi, M.; Maruyama, T.; Muragaki, Y.; Kobayashi, E.; Iseki, H.; Sakuma, I. *Med. Image Anal.* **2012**, *16*, 754-766.
(10) Sahoo, N.; Goradia, N.; Ohlenschlager, O.; Schonherr, R.; Friedrich, M.; Plass, W.; Kappl, R.; Hoshi, T.; Heinemann, S. H. *Proc. Natl. Acad. Sci. U.S.A.* **2013**, *110*, E4036-E4044.
(11) Prabhakar, N. R.; Peers, C. *Physiology* **2014**, *29*, 49-57.
(12) Zhang, J. L.; Kang, Z.; Chen, J.; Du, G. C. *Sci. Rep.* **2015**, *5*, 8584.
(13) Sigala, P. A.; Crowley, J. R.; Henderson, J. P.; Goldberg, D. E. *eLife* **2015**, *4*, doi: 10.7554/eLife.09143.
(14) Li, T.; Wang, E.; Dong, S. *Anal. Chem.* **2010**, *82*, 7576-7580.
(15) Xu, C.-X.; Zheng, Y.-X.; Zheng, X.-H.; Hu, Q.; Zhao, Y.; Ji, L.-N.; Mao, Z.-W. *Sci. Rep.* **2013**, *3*, 2060.